11th ANKARA INTERNATIONAL AEROSPACE CONFERENCE **AIAC-2021-049**
8-10 September 2021 - METU, Ankara TURKEY

PREDICTION OF LINEAR COMBUSTION INSTABILITIES IN ROCKET ENGINES

Musa Onur ÖZTÜRKMEN*†
Middle East Technical University
Roketsan Inc.
Ankara, Turkey

Yusuf ÖZYÖRÜK‡
Middle East Technical University
Ankara, Turkey

ABSTRACT

Pressure oscillations inherently exist in rocket engines due to their high power density associated with turbulent combustion. Coupling of the acoustic eigenmodes of the combustion chamber with the unsteady heat release from combustion may lead to combustion instability which can impose important stresses and vibration on the combustion chamber as well as the whole vehicle. In this paper, an iterative methodology is utilized to predict the onset of combustion instabilities in rocket engines. An experimental combustion chamber from literature is investigated, and the computed results are compared with measure data. The results reveal that the iterative method works reasonably as long as the inhomogeneity due to either boundary conditions or unsteady heat sources is restricted to small values.

INTRODUCTION

Combustion instability can simply be defined as undesired rise of the combustion chamber pressure. This pressure rise leads to important fluctuations in thrust generation as well as stresses and vibration on the structure or even to the destruction of the engine [Searby, 1991; Candel, 2004]. A typical pressure oscillation inside a combustion chamber is shown in Figure 1, as an example.

The pressure inside the combustion chamber is not constant during the operation of a rocket. The pressure may oscillate due to many reasons, such as turbulence, fluctuations in atomization process, even from the propellant supply lines. These oscillations seen due to the nature of rocket engines are not called as combustion instability. However, if such perturbations start developing a positive feedback between the chamber acoustic field and unsteady heat release, then the pressure fluctuations may start rising in an uncontrolled manner, leading to unacceptable levels. Such coupling of the unsteady heat release and increasing acoustic pressure fluctuations is called thermoacoustic instability, commonly termed combustion instability in rocket and air-breathing engines. Therefore, the prediction of combustion instability and its alleviation during the design of a rocket engine is important.

*Graduate Student, Email: onur.ozturkmen@metu.edu.tr
†Lead Engineer, Email: oozturkmen@roketsan.com.tr
‡Prof. in Aerospace Engineering Department, Email: yusuf.ozyoruk@ae.metu.edu.tr

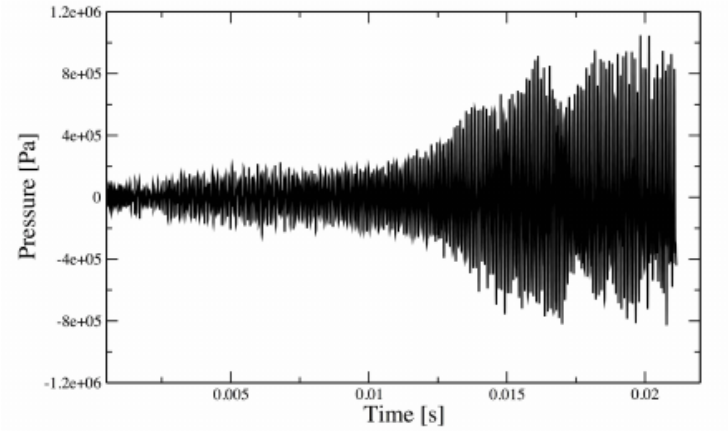

Figure 1: Pressure fluctuations in a LPRE [Schmitt, 2017]

Combustion instability prediction methods can be classified according to their level of accuracy. In low order modelling approach, network models are used [Evesque, 2002], [Stow, 2009]. These models treat the combustion chamber as one dimensional components with discontinuities to model the flame, geometric changes, and so on. Large Eddy Simulation (LES) can be used to resolve not only the combustion dynamics inside the chamber, but also the acoustic behaviour of the chamber. However, this resolution comes with a high computational expense, and it cannot be affordable for real rocket engines. In literature, with LES mostly laboratory scale combustion chamber stability characteristics are investigated [Schmitt, 2017], [Urbano, 2016]. To decrease computational requirements, methods that depend on the linearized equations with finite volume/element discretization or inhomogeneous wave equation are widely used [Culick , 2006], [Nicoud, 2007], [Pieringer, 2009], provided that a model for the interaction of the unsteady heat release and pressure oscillations, commonly called flame transfer function (FTF), is supplied. These methods are then well suited for complex geometries compared to direct use of LES for each specific case. The FTF itself is obtained through either experiments or LES. In any case investigation of combustion instability is a laborious and difficult task.

In this study, the iterative methodology suggested by Culick [2006] is utilized for the prediction of linear combustion instabilities. The method is based on determining the perturbed wavenumbers and eigenmodes of the chamber, and thereby existence of any instability driving coupling between the heat release and acoustics. The details of the iterative method are described in the next section.

PREDICTION OF COMBUSTION INSTABILITY

Wave Equation for a Combustion Chamber

The conservation equations for a two phase mixture in non-conservative form are given by equations (1) - (3). In these equations, the density is defined as the sum of all the phases, i.e. $\rho = \rho_l + \rho_g$.

$$\frac{\partial \rho}{\partial t} + \boldsymbol{u} \cdot \nabla \rho + \rho \nabla \cdot \boldsymbol{u} = \mathscr{W} \tag{1}$$

$$\rho \left[\frac{\partial \boldsymbol{u}}{\partial t} + \boldsymbol{u} \cdot \nabla \boldsymbol{u} \right] = -\nabla p + \mathcal{F} \tag{2}$$

$$\rho C_v \left[\frac{\partial T}{\partial t} + \boldsymbol{u} \cdot \nabla T + p \nabla \cdot \boldsymbol{u} \right] = \mathcal{Q} \tag{3}$$

where, $\mathscr{W}$, $\mathcal{F}$, and $\mathcal{Q}$ represent the mass, momentum and energy source terms, respectively. A detailed explanation of the conservation equations and source terms can be found in Culick [2006].

The wave equation for a combustion chamber, which accounts for the terms related to combustion processes such as evaporation, heat release and so on, can be derived following the same procedure as that of the classical acoustics. The wave equation for a generic combustion chamber, after writing any instantaneous variable Q as the summation of its time mean plus a fluctuating part about it, i.e. $Q = Q_0 + Q'$, is obtained first by taking the divergence of the momentum equation and time derivative of the pressure equation (combination of the continuity and energy equation), and then subtracting the resultant equations from each other. After some further manipulations, the wave equation and the corresponding boundary condition are given by equation (4).

$$\begin{aligned} \nabla^2 p' - \frac{1}{\bar{c}^2}\frac{\partial^2 p'}{\partial t^2} &= h, \quad \text{in } \mathcal{V} \\ \hat{\boldsymbol{n}} \cdot \nabla p' &= -f, \quad \text{on } \mathcal{S} \end{aligned} \tag{4}$$

where, p' is the pressure perturbation, $\bar{c}$ represents the chamber averaged speed of sound, h signifies the volume ($\mathcal{V}$) source terms that arise from the coupling between acoustics and combustion, and f includes the effects of the chamber boundary ($\mathcal{S}$) conditions, $\hat{\boldsymbol{n}}$ is the boundary unit normal vector. The interaction between acoustics and combustion is shown schematically in Figure 2.

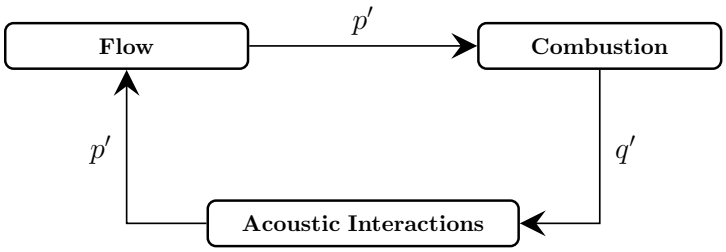

Figure 2: The interaction between acoustics and combustion

The boundary conditions represented by the source term f account for acoustic losses due to impedance of the chamber walls and nozzle, as well as interactions with the injector. The source term h, which behaves as a gain mechanism for the instability, includes linear and non-linear gas dynamic effects, the entropy fluctuation effects and terms related to the combustion process such as evaporation, heat release and so on. The most important contribution from these terms comes from the combustion process for the liquid propellant rocket engines. The other terms can be neglected [Culick , 2006] since the mean flow inside the chamber is small compared to speed of sound and the chamber geometries are generally short.

Solution of the Wave Equation

Assuming the time dependency of any fluctuating quantity $Q'(\boldsymbol{x}, t)$ in the form $\sum_\omega \hat{Q}(\boldsymbol{x}, \omega)e^{i\omega t}$, where ω is the angular frequency of oscillation, we can write the inhomogeneous wave equation, equation (4), (for brevity frequency dependence of p is not shown explicitly)

$$\begin{aligned} \nabla^2 \hat{p}(\boldsymbol{x}) + k^2 \hat{p}(\boldsymbol{x}) &= \hat{h}(\boldsymbol{x}), \quad \text{in } \mathcal{V} \\ \hat{\boldsymbol{n}}(\boldsymbol{x}) \cdot \nabla \hat{p}(\boldsymbol{x}) &= -\hat{f}(\boldsymbol{x}), \quad \text{on } \mathcal{S} \end{aligned} \tag{5}$$

where $k = \omega/\bar{c}$ is the wave number. The normal acoustic modes $\hat{p}_N$ of a combustion chamber can be obtained by solving the homogeneous wave equation given by

$$\begin{aligned} \nabla^2 \hat{\psi}_N(\boldsymbol{x}) + k_N^2 \hat{\psi}_N(\boldsymbol{x}) &= 0, \quad \text{in } \mathcal{V} \\ \hat{\boldsymbol{n}}(\boldsymbol{x}) \cdot \nabla \hat{\psi}_N(\boldsymbol{x}) &= 0, \quad \text{on } \mathcal{S} \end{aligned} \tag{6}$$

where $\hat{\psi}_N \equiv \hat{p}_N$ and k_N represent the normal mode shapes and wave numbers, respectively. Note that the normal mode angular frequencies ω_N are written in terms of the wave number and mean speed of sound as $\omega_N = \bar{c}k_N$.

Multiplying equation (5) by $\hat{\psi}_N$ and equation (6) by $\hat{p}$, then subtracting from each other and then integrating the resulting equation over the chamber volume $\mathcal{V}$ bounded by surface $\mathcal{S}$, one can obtain

$$k^2 - k_N^2 = \frac{1}{\int\limits_{\mathcal{V}} \hat{\psi}_N(\boldsymbol{x})\hat{p}(\boldsymbol{x})\, d\mathcal{V}} \left\{ \int\limits_{\mathcal{V}} \hat{\psi}_N(\boldsymbol{x})\hat{h}(\boldsymbol{x})\, d\mathcal{V} + \int\limits_{S} \hat{\psi}_N(\boldsymbol{x})\hat{f}(\boldsymbol{x})\, d\mathcal{S} \right\}. \tag{7}$$

Using the Green's function and its properties, the perturbed mode functions, $\hat{p}$, can be defined as a series expansion of the normal mode shapes $\hat{\psi}_N$. Recognizing that the normal modes are the solution of the homogeneous problem and are therefore orthogonal, the Green function can be written as follows:

$$\hat{G}(\boldsymbol{x}|\boldsymbol{y}) = \sum_{\boldsymbol{\ell}=0}^{\infty} \frac{\hat{\psi}_{N,\boldsymbol{\ell}}(\boldsymbol{x})\hat{\psi}_{N,\boldsymbol{\ell}}(\boldsymbol{y})}{E_{\boldsymbol{\ell}}^2(k^2 - k_{N,\boldsymbol{\ell}}^2)} \quad \text{with} \quad E_{\boldsymbol{\ell}}^2 \delta_{\boldsymbol{\ell}\boldsymbol{m}} = \int\limits_{\mathcal{V}} \hat{\psi}_{N,\boldsymbol{\ell}}(\boldsymbol{x})\hat{\psi}_{N,\boldsymbol{m}}(\boldsymbol{x})\, d\mathcal{V} \tag{8}$$

where the subscript N to $\hat{\psi}$ and k indicates the associated quantity is that of the natural mode, and the bold subscript $\boldsymbol{\ell}$ or $\boldsymbol{m}$ indicates the array of the mode indices in the directions of the dimensionality of the problem, such as the first longitudinal, second transverse mode, and so on. Taking convolution of the inhomogeneous wave equation, equation (5), with Green function (8), one can find:

$$\hat{p}(\boldsymbol{x}) = \sum_{\boldsymbol{\ell}=0}^{\infty} \frac{\hat{\psi}_{N,\boldsymbol{\ell}}(\boldsymbol{x})}{E_{\boldsymbol{\ell}}^2(k^2 - k_{N,\boldsymbol{\ell}}^2)} \left\{ \int_{\mathcal{V}(\boldsymbol{y})} \hat{\psi}_{N,\boldsymbol{\ell}}(\boldsymbol{y})\hat{h}(\boldsymbol{y})\, d\mathcal{V}(\boldsymbol{y}) + \int_{\mathcal{S}(\boldsymbol{y})} \hat{\psi}_{N,\boldsymbol{\ell}}(\boldsymbol{y})\hat{f}(\boldsymbol{y})\, d\mathcal{S}(\boldsymbol{y}) \right\}. \tag{9}$$

Since the solutions of the perturbed modes should approach to the normal mode solutions as the source terms, $\hat{h}$ and $\hat{f}$, go to zero, one can write the following relations:

$$k_{\boldsymbol{\ell}}^2 = k_{N,\boldsymbol{\ell}}^2 + \frac{1}{E_{\boldsymbol{\ell}}^2} \left\{ \int_{\mathcal{V}(\boldsymbol{y})} \hat{\psi}_{N,\boldsymbol{\ell}}(\boldsymbol{y})\hat{h}(\boldsymbol{y})\, d\mathcal{V}(\boldsymbol{y}) + \int_{\mathcal{S}(\boldsymbol{y})} \hat{\psi}_{N,\boldsymbol{\ell}}(\boldsymbol{y})\hat{f}(\boldsymbol{y})\, d\mathcal{S}(\boldsymbol{y}) \right\} \tag{10}$$

$$\hat{p}_{\boldsymbol{\ell}}(\boldsymbol{x}) = \psi_{N,\boldsymbol{\ell}}(\boldsymbol{x}) + \sum_{\boldsymbol{m}=0}^{\infty} \frac{\hat{\psi}_{N,\boldsymbol{m}}(\boldsymbol{x})(1 - \delta_{\boldsymbol{\ell}\boldsymbol{m}})}{E_{\boldsymbol{m}}^2(k_{\boldsymbol{\ell}}^2 - k_{N,\boldsymbol{m}}^2)} \left\{ \int_{\mathcal{V}(\boldsymbol{y})} \hat{\psi}_{N,\boldsymbol{m}}(\boldsymbol{y})\hat{h}(\boldsymbol{y})\, d\mathcal{V}(\boldsymbol{y}) + \int_{\mathcal{S}(\boldsymbol{y})} \hat{\psi}_{N,\boldsymbol{m}}(\boldsymbol{y})\hat{f}(\boldsymbol{y})\, d\mathcal{S}(\boldsymbol{y}) \right\} \tag{11}$$

where

$$E_{\boldsymbol{m}}^2 = \int_{\mathcal{V}} \hat{\psi}_{N,\boldsymbol{m}}^2\, d\mathcal{V}. \tag{12}$$

Equations (10) and (11) form an implicit system for the solution of the perturbed, inhomogeneous problem, because $\hat{f}$ and $\hat{h}$ are both functions of the perturbed solution. The solution for the perturbed mode structures can be obtained using an iterative methodology [Culick , 1995]. The right-hand sides of equations (10) and (11) are computed with the available mode shape functions and wavenumbers where the infinite sum is replaced with a finite one. The computations are started with an initial condition of

$$\hat{p}_{\boldsymbol{\ell}} = \hat{\psi}_{N,\boldsymbol{\ell}}, \quad k_{\boldsymbol{\ell}} = k_{N,\boldsymbol{\ell}}, \tag{13}$$

Although the solution procedure by the iterative method is simple, there is a condition for the convergence that is the source terms should be small. Another requirement for thermoacoustic instability analysis to obtain the source term $\hat{h}$ due to combustion. Determination of the unsteady heat release distribution inside the chamber is not an easy task. The heat release rate can be found experimentally or using numerical method like LES.

Treatment of Unsteady Heat Release

The source of thermoacoustic instability is the unsteady heat release coupled with chamber acoustics in a way that drives the pressure perturbations to higher levels. A common way of treating the heat source in the inhomogeneous wave equation is to link the heat source with pressure fluctuations, by defining a flame transfer function (FTF) based on the axial velocity fluctuation $\hat{u}$ at $\boldsymbol{x}_{\mathrm{ref}}$, a reference coordinate, in the form :

$$\mathrm{FTF} = R_{\hat{q}\hat{u}_{\mathrm{ref}}}(\boldsymbol{x}) = \frac{\hat{q}(\boldsymbol{x})}{\hat{u}(\boldsymbol{x}_{\mathrm{ref}})} \tag{14}$$

There are two possibilities to define the velocity fluctuation in this expression. One is through the use of the local impedance at the reference point. The other one is to use the axial momentum equation. The former requires the explicit knowledge of the impedance at the reference point, while the latter requires solution of the velocity fluctuation at that point.

Using the local impedance one can express the velocity fluctuation as

$$\hat{u}(\boldsymbol{x}_{\mathrm{ref}}) = \frac{\hat{p}(\boldsymbol{x}_{\mathrm{ref}})}{\bar{\rho}\bar{c}Z^*(\boldsymbol{x}_{\mathrm{ref}})} = \frac{\hat{p}(\boldsymbol{x}_{\mathrm{ref}})A^*(\boldsymbol{x}_{\mathrm{ref}})}{\bar{\rho}\bar{c}} \tag{15}$$

FTF may also be written as

$$\hat{R}_{\hat{q}\hat{u}_{\mathrm{ref}}} = n(\boldsymbol{x})e^{-i\omega\tau(\boldsymbol{x})} \tag{16}$$

where $n(\boldsymbol{x})$ is called the interaction index, and $\tau(\boldsymbol{x})$ is called the time delay. Both are in general dependent on the frequency of oscillations.

From the linearized x-momentum equation the axial velocity fluctuation and pressure perturbation are related by

$$\hat{u}(\boldsymbol{x}_{\mathrm{ref}}) = -\frac{\nabla\hat{p}(\boldsymbol{x}_{\mathrm{ref}})}{i\bar{\rho}\bar{c}k} \tag{17}$$

In this way the heat source term appearing in the inhomogeneous Helmholtz equation becomes

$$\begin{aligned}\hat{h} = -\frac{\gamma-1}{\bar{c}}ik\hat{q} &= -\frac{\gamma-1}{\bar{\rho}\bar{c}^2}ik\hat{R}_{\hat{q}\hat{u}_{\mathrm{ref}}}\hat{p}(\boldsymbol{x}_{\mathrm{ref}})A^*_{\mathrm{ref}}, \text{ or} \\ &= \frac{\gamma-1}{\bar{\rho}\bar{c}^2}\hat{R}_{\hat{q}\hat{u}_{\mathrm{ref}}}\nabla\hat{p}(\boldsymbol{x}_{\mathrm{ref}})\end{aligned} \tag{18}$$

Treatment of Impedance Boundary

When a boundary of the chamber has finite impedance, that is the boundary transmits part of the acoustic energy, the proper condition to impose there, using the impedance definition given by equation (15) and the normal momentum equation, is

$$-\hat{\boldsymbol{n}}(\boldsymbol{x})\cdot\nabla\hat{p}(\boldsymbol{x})|_{\mathcal{S}} = ikA^*(\boldsymbol{x})\hat{p}(\boldsymbol{x})|_{\mathcal{S}} \equiv \hat{f} \tag{19}$$

Evaluation of Stability

In this paper the iterative approach is used to predict the onset of the instabilities, i.e. linear instabilities inside the chamber. The source terms determine the net energy balance between the energy addition into combustion chamber due to heat release and the acoustic energy losses due to the impedance of the nozzle and injector. Depending on this net balance, the pressure oscillations inside the chamber will grow or decay with time. The sign of the imaginary part of the wave number of the inhomogeneous problem will determine whether an acoustic mode is linearly stable or not.

RESULTS AND DISCUSSION

In this section the iterative analysis approach to solving the inhomogeneous wave equation with internal and boundary sources is tested with two different cases. The first is a simple problem for which analytical solution can be obtained. It is a two dimensional rectangular geometry with an impedance boundary condition applied at the right boundary. The second problem is a laboratory combustor case known as Continuously Variable Resonance Chamber (CVRC) [Miller, 2005; Yu, 2009] for which a LES computed flame transfer function and stability analysis results are available [Garby, 2013]. These cases are discussed below.

Case 1: 2D Rectangular Geometry with impedance boundary condition

The rectangular domain has a length of L and height of H. All wall boundaries except the right one is rigid. Finite impedance boundary condition is imposed on the right wall, which changes the mode structures from the natural ones. The schematic of the problem is shown in Figure 3.

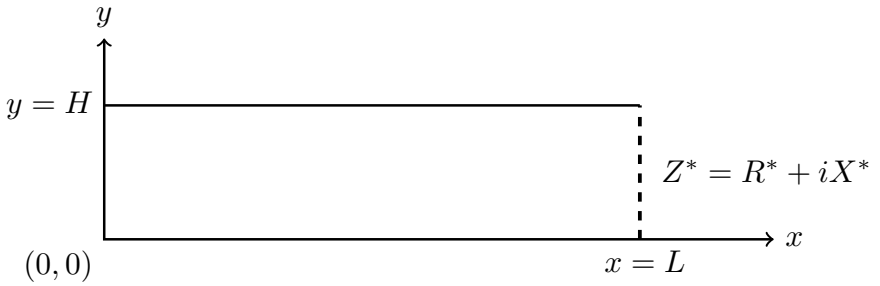

Figure 3: 2D rectangular domain with impedance boundary condition

This problem is chosen as a verification case as both the natural modes and perturbed modes with one boundary or two boundaries given in a direction may be treated with finite impedance to which analytical solutions can be obtained. The two dimensional problem is setup with a length of $L = 1$ m in the x, and a height of $H = 0.25$ m in the y-directions, respectively. The medium inside the domain is assumed as stagnant air where the speed of sound and density values are set to $\bar{c} = 340$ m/s and $\bar{\rho} = 1.225$ kg/m^3, respectively. While the internal source $\hat{h}$ is taken zero, the boundary condition with a finite impedance value at the right wall is formulated using the x-momentum equation, as has been expressed above by equation (19).

The iterations are initiated using the natural mode shapes and wavenumbers, which are the solutions to the homogeneous problem, $\hat{f} = \hat{h} = 0$, and given by

$$\hat{\psi}_{N,\boldsymbol{\ell}=(l,n)}(x,y) = \cos\big(\frac{\pi l x}{L}\big)\cos\big(\frac{\pi n y}{H}\big), \quad k_{N,\boldsymbol{\ell}} = \sqrt{\big(\frac{\pi l}{L}\big)^2 + \big(\frac{\pi n}{H}\big)^2}, \quad l = 0, 1, 2, ..., \; n = 0, 1, 2, ... \tag{20}$$

Calculations with the right boundary allowing passage of acoustic energy and thereby exhibiting inhomogeneity are carried out for the two different impedance values of $Z^* = 4 - 4i$, and $Z^* = 0.5 - 0.5i$, respectively. The solutions for various modes are presented in forms of analytically obtained natural modal shapes and wavenumbers, perturbed modal shapes and wavenumbers, and iteratively found perturbed modal shapes and wavenumbers. An impedance boundary allows transmission of wave energies, and hence is expected to yield positive imaginary parts for the perturbed wavenumbers.

The infinite sum term of equation (11) was replaced by a finite sum with $N_l = 4$ longitudinal and $N_n = 2$ transverse modes. The iterative solutions are given in Figure 4, and Table 1 for $Z^* = 4 - 4i$, and in Figure 5 and Table 2 for $Z^* = 0.5 - 0.5i$, respectively. In the tables the natural wavenumbers are indicated by k_N, the perturbed exact wavenumbers by k_{exact}, and the iteratively calculated ones by k_{iter}. The mode indices are indicated by $\boldsymbol{\ell} = (l, n)$ for oscillations in the axial and transverse directions, respectively. It is clear that the analytical solutions have positive imaginary parts for the wavenumbers as expected. It is also evident from the results that the higher one of the two

impedance values tested resulted for a large range of mode numbers reasonably good agreement with the analytical ones, but this statement is not true for all the modal contents of the waves at the lower impedance value. The pressure contours of the modes (modal shapes) appear to be relatively more sensitive to the imaginary parts of the resulting wavenumbers. As pointed out earlier that the success of the iterative approach relies on how small the source terms in the inhomogeneous wave equation are. Since the boundary source term $\hat{f}$ is inversely proportional to the impedance Z^*, lowering it caused larger inhomogeneity. In such cases a more direct approach to solving the Helmholtz equation appears as a necessity.

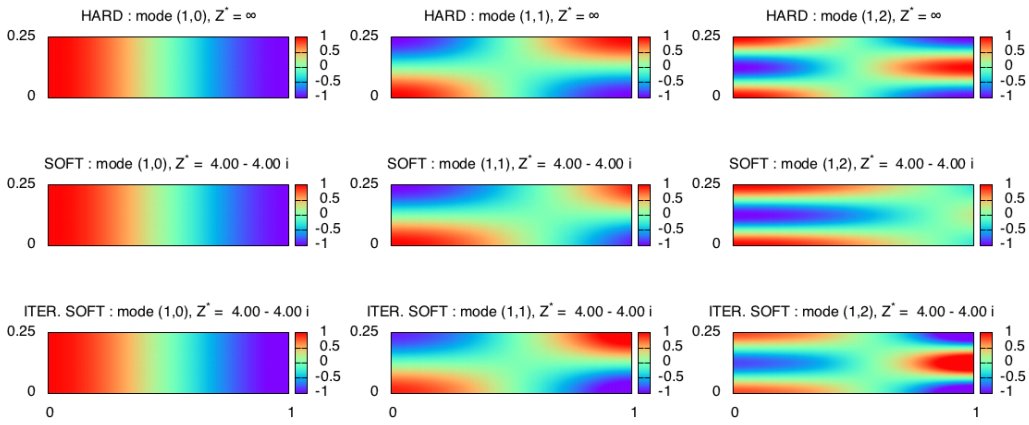

(a) Mode (1,0) (b) Mode (1,1) (c) Mode (1,2)

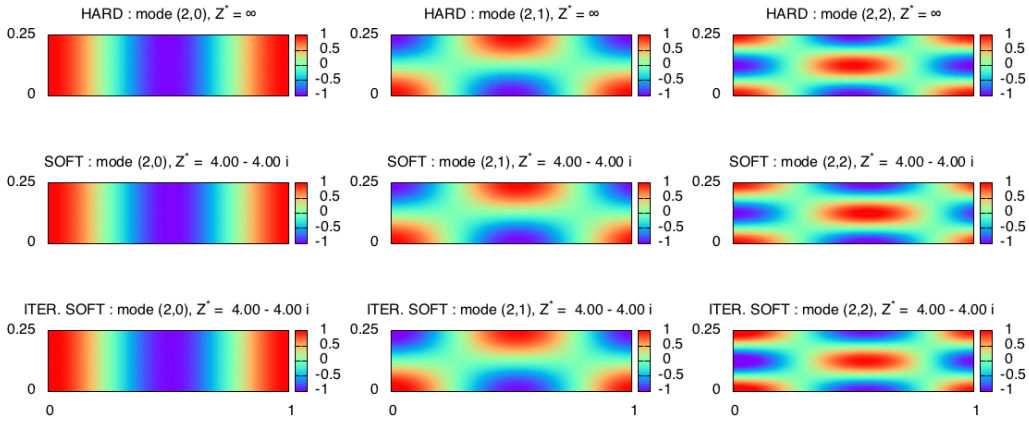

(d) Mode (2,0) (e) Mode (2,1) (f) Mode (2,2)

Figure 4: Mode shapes for $Z^* = 4 - 4i$

Case 2: CVRC test case

In this section the experimental setup from literature called as Continuously Variable Resonance Chamber (CVRC) [Miller, 2005], [Yu, 2009], [Sisco, 2011] is used as a validation case with the chamber volume with LES computed heat sources as well as the chamber outlet opening to the nozzle with an impedance condition. The combustion chamber is a cylindrical body, which has dimensions of 38.1 cm in length and 4.5 cm in diameter. The fuel and oxidizer are introduced into the combustion chamber by a coaxial injector. The oxidizer post length may be varied between 8.89 cm and 19.05 cm. Due to this post length the combustion chamber exhibits different stability characteristics resulting from the interactions of the combustion in the chamber and its acoustic field as well as that developing through the post oxidizer cavity. The numerical study is conducted with 12.065 cm post length. The combustion chamber is finalized with a converging diverging nozzle to limit the mass flow and hence build a desired level of pressure inside the chamber. The dimensions of the geometry used in this study are shown in Figure 6. Further details of the geometry of the

Table 1: The wave number solutions for $Z^* = 4 - 4i$, $N_l = 4$, $N_n = 2$.

$\boldsymbol{\ell} = (l, n)$	$k_{N,\boldsymbol{\ell}}$ [1/m]	$k_{\text{exact},\boldsymbol{\ell}}$ [1/m]	$k_{\text{iter},\boldsymbol{\ell}}$ [1/m]	$f_{\text{iter},\boldsymbol{\ell}}/f_{N,\boldsymbol{\ell}}$ [-]	Z^*
$(1,0)$	3.142	$(3.015, 0.124)$	$(3.016, 0.130)$	0.960	$(4.00, -4.00)$
$(2,0)$	6.283	$(6.157, 0.124)$	$(6.157, 0.120)$	0.980	$(4.00, -4.00)$
$(3,0)$	9.425	$(9.299, 0.124)$	$(9.300, 0.112)$	0.987	$(4.00, -4.00)$
$(4,0)$	12.566	$(12.440, 0.124)$	$(12.443, 0.102)$	0.990	$(4.00, -4.00)$
$(1,1)$	12.953	$(12.792, 0.121)$	$(12.830, 0.170)$	0.991	$(4.00, -4.00)$
$(2,1)$	14.050	$(13.918, 0.123)$	$(13.920, 0.114)$	0.991	$(4.00, -4.00)$
$(3,1)$	15.708	$(15.579, 0.123)$	$(15.582, 0.105)$	0.992	$(4.00, -4.00)$
$(4,1)$	17.772	$(17.644, 0.123)$	$(17.649, 0.094)$	0.993	$(4.00, -4.00)$
$(1,2)$	25.328	$(25.197, 0.024)$	$(25.209, 0.225)$	0.995	$(4.00, -4.00)$
$(2,2)$	25.906	$(25.759, 0.105)$	$(25.769, 0.096)$	0.995	$(4.00, -4.00)$
$(3,2)$	26.842	$(26.706, 0.117)$	$(26.716, 0.089)$	0.995	$(4.00, -4.00)$
$(4,2)$	28.099	$(27.968, 0.120)$	$(27.981, 0.080)$	0.996	$(4.00, -4.00)$

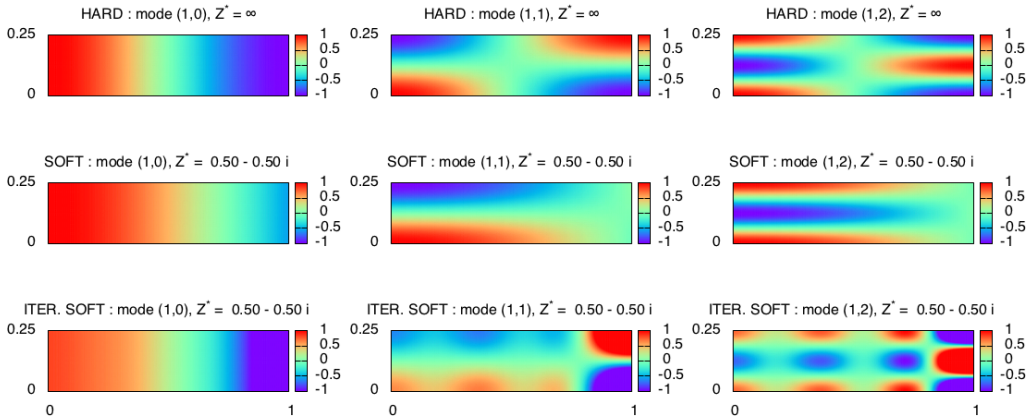

(a) Mode (1,0) (b) Mode (1,1) (c) Mode (1,2)

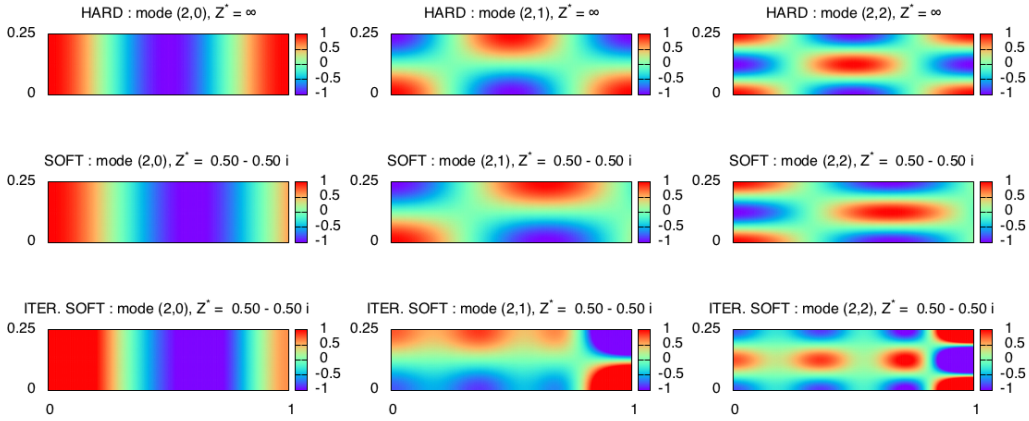

(d) Mode (2,0) (e) Mode (2,1) (f) Mode (2,2)

Figure 5: Mode shapes for $Z^* = 0.5 - 0.5i$

experimental set-up can be found in Yu [2009]. The fuel composition is pure gaseous methane. The oxidizer is a gaseous mixture composed of 42% oxygen and 58% water in terms of mass fraction. The oxidizer and fuel are injected into chamber at 1030 K and 300 K, respectively.

The chamber volume averaged gas properties are provided in Table 3. In order to account for more realistic impedance values at the outlet of the combustion chamber or nozzle inlet, the frequency-domain linearized Euler equations were solved in one dimension (in the axial direction) numerically with a backward differencing starting from the nozzle throat where due to flow choking the impedance

Table 2: The wave number solutions for $Z^* = 0.5 - 0.5i$.

$\boldsymbol{\ell} = (l, n)$	$k_{N,\boldsymbol{\ell}}$ [1/m]	$k_{\text{exact},\boldsymbol{\ell}}$ [1/m]	$k_{\text{iter},\boldsymbol{\ell}}$ [1/m]	$f_{\text{iter},\boldsymbol{\ell}}/f_{N,\boldsymbol{\ell}}$ [-]	Z^*
$(1, 0)$	3.142	$(2.124, 0.402)$	$(1.673, -1.356)$	0.532	$(0.50, -0.50)$
$(2, 0)$	6.283	$(5.266, 0.402)$	$(6.460, 0.502)$	1.028	$(0.50, -0.50)$
$(3, 0)$	9.425	$(8.408, 0.402)$	$(8.212, 1.417)$	0.871	$(0.50, -0.50)$
$(4, 0)$	12.566	$(11.549, 0.402)$	$(6.108, 4.537)$	0.486	$(0.50, -0.50)$
$(1, 1)$	12.953	$(12.672, 0.009)$	$(10.644, 2.618)$	0.822	$(0.50, -0.50)$
$(2, 1)$	14.050	$(13.484, 0.067)$	$(10.465, 2.476)$	0.745	$(0.50, -0.50)$
$(3, 1)$	15.708	$(14.967, 0.144)$	$(14.895, 0.782)$	0.948	$(0.50, -0.50)$
$(4, 1)$	17.772	$(16.931, 0.210)$	$(10.166, -3.165)$	0.572	$(0.50, -0.50)$
$(1, 2)$	25.328	$(25.184, 0.002)$	$(22.395, 3.275)$	0.884	$(0.50, -0.50)$
$(2, 2)$	25.906	$(25.588, 0.018)$	$(22.391, 3.281)$	0.864	$(0.50, -0.50)$
$(3, 2)$	26.842	$(26.377, 0.046)$	$(22.520, 3.314)$	0.839	$(0.50, -0.50)$
$(4, 2)$	28.099	$(27.515, 0.082)$	$(19.474, 3.312)$	0.693	$(0.50, -0.50)$

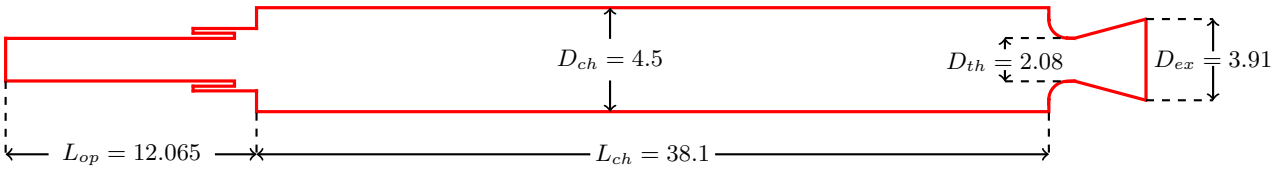

Figure 6: Geometry of the CVRC (dimensions are in cm)

was set, with $\exp(+i\omega t)$ dependence, to

$$\frac{Z}{\rho_0 c_0}\Big|_{\text{throat}} = Z^*|_{\text{throat}} = \frac{2\frac{du_0}{dx} + i\omega}{(\gamma - 1)\frac{du_0}{dx} + i\omega}\Big|_{\text{throat}} \tag{21}$$

where u_0 is the mean axial velocity through the nozzle which was calculated based on the 1-D ideal gas dynamics relations. The computed impedance values for the nozzle inlet boundary are shown in Figure 7. It is clear that at low frequencies the impedance values are high, and hence the first a couple of longitudinal modes are expected to have significant reflection from the chamber outlet boundary. For these modes the iterative method is expected to work well with the boundary inhomogeneity.

Table 3: Chamber averaged gas properties in CVRC setup.

T [K]	p [MPa]	T_{tot} [K]	p_{tot} [MPa]	γ	R [J/kgK]
2512	1.54	2526.29	1.598	1.182	389.2

To test the iterative algorithm quickly against the outlet impedance condition, a 2-D rectangular geometry with the length of the CVRC chamber, and height of the CVRC diameter was considered. Although the CVRC chamber is of cylindrical shape, the results for pure longitudinal modes do not get altered in absence of volumetric (heat) sources. 2-D calculations with heat sources could still be performed, but by taking the actual volume weighting into account properly (i.e. radius effect). The computed wavenumbers for the 2-D rectangular shape are shown in Table 4. It is clear that the outlet impedance condition changed the wavenumbers only slightly from the those of the natural modes.

Now in this part of the numerical study, the FTF given graphically in the study of Garby [2013] is modelled by a functional fit, and then incorporated into the iterative solution approach as the volume heat source, given by equation (18), in addition to the sources due to the outlet and inlet impedance conditions (19). The FTF is defined based on the axial velocity fluctuation $\hat{u}$ at $\boldsymbol{x}_{\text{ref}} = (x, r) = (0, 0)$,

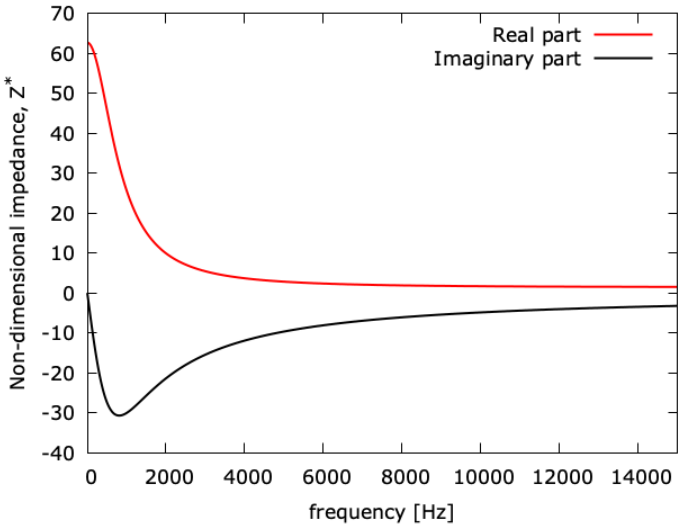

Figure 7: CVRC nozzle inlet impedance.

Table 4: Wavenumbers of longitudinal modes in CVRC chamber with frequency-dependent impedance, $Z_2^* = Z_2^*(f)$ at the outlet boundary, i.e. $\hat{f} \neq 0$, $\hat{h} = 0$, $N_l = 5, N_n = 2$.

$\boldsymbol{\ell} = (l, n)$	$k_{N,\boldsymbol{\ell}}$ [1/m]	$k_{\text{exact},\boldsymbol{\ell}}$ [1/m]	$k_{\text{iter},\boldsymbol{\ell}}$ [1/m]	$\text{Re}(f_{\text{iter},\boldsymbol{\ell}})$ [Hz]	$Z_2^*(f)$
$(1, 0)$	8.267	$(8.196, 0.044)$	$(8.192, 0.055)$	1401.5	$(16.66, -26.64)$
$(2, 0)$	16.535	$(16.393, 0.052)$	$(16.394, 0.050)$	2804.8	$(5.98, -16.39)$
$(3, 0)$	24.802	$(24.591, 0.063)$	$(24.604, 0.051)$	4209.4	$(3.43, -11.40)$
$(4, 0)$	33.069	$(32.790, 0.080)$	$(32.822, 0.051)$	5615.4	$(2.50, -8.67)$

which is the reference coordinate used in FTF processing, the injector exit at the chamber centerline. The LES computed FTF results of Garby [2013] and their functional fits are given in Figure 8. The fits shown in the bottom row of this figure were obtained approximately from the contour plot levels given in the top row of the figure. In the computations, the interaction index $n(\boldsymbol{x})$ and time delay $\tau(\boldsymbol{x})$ levels (refer to equation (16) for the definition of FTF) shown in the fits were scaled to match the global interaction index $n_g = 10525$ J/m, and global time delay $\tau_g = 2.89 \times 10^{-4}$ s values of [Garby, 2013]. The global values are volume integrated values:

$$n_g e^{-i\omega\tau_g} = \int_{\mathcal{V}} n(\boldsymbol{x}) e^{-i\omega\tau(\boldsymbol{x})}\, d\mathcal{V} \tag{22}$$

The reference velocity fluctuation required for the computations with FTF is assumed to be given by equation (15), which in turn requires the impedance at the reference point. Since in the computations the domain is assumed to start from the injector location, the reference point impedance and the impedance of the open part of the inlet boundary are the same and equal to $Z_1^* = 1/A_1^*$ (see Figure 9). In the computations its value is taken as fixed at $Z_1^* = 3.3$ [Garby, 2013]. On the other hand the outlet impedance $Z_2^* = 1/A_2^*$ needed for the outlet condition (Figure 9) is taken as frequency-dependent. The outlet impedance is shown in Figure 7.

In the experiments the chamber inlet and outlet experience small velocities. Therefore, along with the default assumption of no flow at the boundaries, the slight modification introduced by the local flow to the impedance is taken into account by relating the fluctuating axial velocity and pressure using the convected momentum equation. This brings a correction to the impedance given by the following expression:

$$\frac{1}{Z_{\text{corr}}^*} = A_{\text{corr}}^* = A^* + \boldsymbol{M} \cdot \hat{\boldsymbol{n}} \tag{23}$$

where Z_{corr}^* is the corrected dimensionless impedance, $\boldsymbol{M}$ is the mean flow Mach number and $\hat{\boldsymbol{n}}$ is

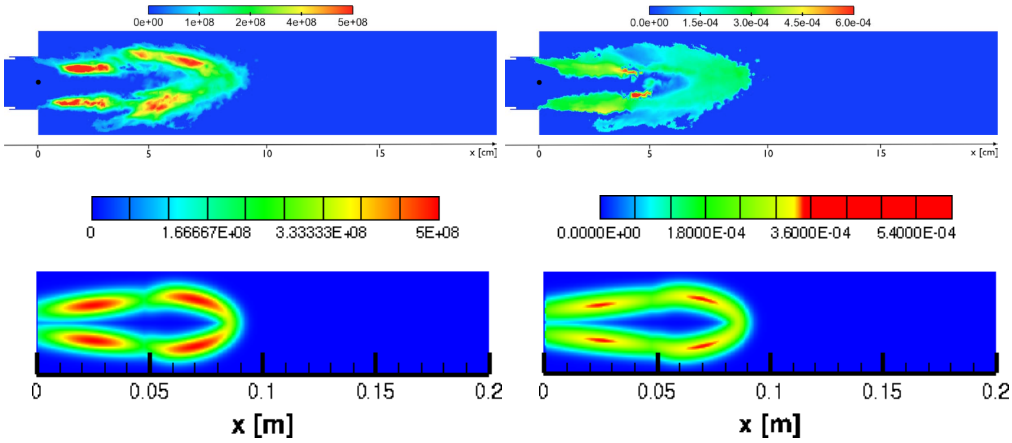

Figure 8: Flame transfer function for the CVRC chamber – interaction index and time delay distributions, as defined in Ref. [Garby, 2013] as FTF $= n(\boldsymbol{x})e^{i\omega\tau(\boldsymbol{x})}$. Top : LES results of Ref. [Garby, 2013] - left: $n(\boldsymbol{x})$, right: $\tau(\boldsymbol{x})$, bottom : Function fit to LES results - - left: $n(\boldsymbol{x})$, right: $\tau(\boldsymbol{x})$. Both are scaled to match the global values of Ref. [Garby, 2013] in the computations.

the unit normal at the boundary. An interpretation of the correction term may be that the flow out of the boundary helps transmission of the outgoing waves. The entire boundary conditions applied in the iterative procedure is shown in Figure 9. The flow Mach numbers at the inlet and outlet during the experiments were $M_1 = 0.32$ and $M_2 = 0.18$, respectively [Garby, 2013].

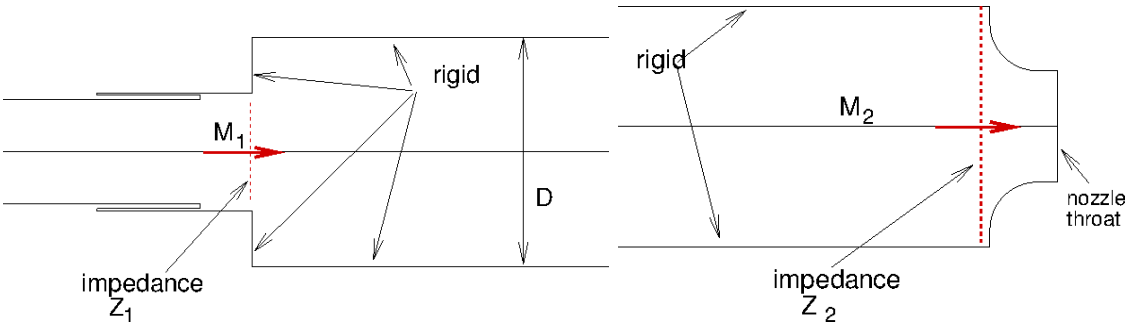

Figure 9: Treatment of the CVRC combustion chamber inlet and outlet boundaries in the iterative solution.

Iterations are started from the natural modes for the closed cylindrical chamber which are given by

$$\hat{\psi}_{N,\boldsymbol{\ell}}(x,r,\theta) = \cos\left(\frac{\pi l x}{L}\right)\,\cos(m\theta)\,J_m(k_{r,mn}r) \tag{24}$$

where (x, r, θ) represent the cylindrical polar coordinates, l is the longitudinal mode index, m is the azimuthal mode index, n is the radial mode index, J_m is the m-th order Bessel function of the first kind, and $k_{r,mn}R$ is the n-th eigenvalue (root) of the equation resulting from the rigid wall condition applied at the chamber surface radius R,

$$\hat{\boldsymbol{n}} \cdot \nabla\hat{\psi}|_{r=R} = 0 \quad \therefore \quad \frac{dJ_m(k_r r)}{dr}\Big|_{r=R} = 0. \tag{25}$$

$\boldsymbol{\ell} = (1, 0, 0)$ is the plane wave mode propagating in the x-direction. The natural wavenumber is obtained from the dispersion relation:

$$k^2_{N,\boldsymbol{\ell}} = \left(\frac{\pi l}{L}\right)^2 + k^2_{r,mn} \tag{26}$$

The computed wavenumbers by the iterative approach using the first $N_l = 20$ longitudinal modes in the sum term of equation (11) are shown in Table 5 without the inlet and outlet flow effects, and in Table 6 with the boundary flow effects. Despite the FTF is not necessarily independent of the modes (frequency), the same interaction index n and time delay τ distributions given in Figure 8 were used for all on the right hand side of equation (11), since no other information was available for FTF. Also included in the tables are the natural and exact wavenumbers that contain only the boundary impedance effects. It is evident from the tables that the heat source resulted a significant effect on the chamber resonance frequencies. By including the unsteady heat release the first mode's frequency increased from only the impedance included value of 1401.5 Hz (see Table 4) to 1483.0 Hz in the case of $M_1 = M_2 = 0$, and to 1514.7 Hz in the case of $M_1 = 0.32$ and $M_2 = 0.18$. Notice that due to consideration of the unsteady heat release $\hat{h}$ the first and third modes have become unstable, as their perturbed wavenumbers have negative imaginary components. The iteratively computed frequency of the first longitudinal mode is in line with other studies, as shown in Table 7. It is particularly interesting to observe in this table that the iteratively found frequency and Garby's LES predicted frequency for the first mode match quite well, despite the use of the same FTF for all the modes involved in the sum term of equation (11). This may be an indication to that the LES predicted FTF is really nearly independent of the frequency for this case. A few additional calculations with varying number of longitudinal modes in the summation in equation (11) were also performed to see whether these were converged results or not. The frequencies calculated are shown in Figure 10 as a function of the number of longitudinal modes included in sum of equation (11). It is evident that first a few modes were sufficient to yield a convergent solution.

Table 5: Stability analysis by the iterative approach for the CVRC configuration with heat and boundary sources, i.e. $\hat{f} \neq 0$, $\hat{h} \neq 0$, $M_1 = 0, M_2 = 0$. $N_l = 20$.

$\boldsymbol{\ell} = (l, m, n)$	$k_{N,\boldsymbol{\ell}}$ [1/m]	$k_{\text{exact},\boldsymbol{\ell}}$ [1/m], $\hat{h} = 0$	$k_{\text{iter},\boldsymbol{\ell}}$ [1/m]	$f_{\text{iter},\boldsymbol{\ell}}$ [Hz]	$Z_2^*(f)$
$(1, 0, 0)$	8.246	$(8.175, 0.954)$	$(8.668, -1.048)$	1483.0	$(15.40, -25.87)$
$(2, 0, 0)$	16.491	$(16.350, 0.961)$	$(16.285, 0.159)$	2786.2	$(6.03, -16.49)$
$(3, 0, 0)$	24.737	$(24.527, 0.973)$	$(24.532, -0.266)$	4197.2	$(3.44, -11.42)$

Table 6: Stability analysis by the iterative approach for the CVRC configuration with heat and boundary sources, i.e. $\hat{f} \neq 0$, $\hat{h} \neq 0$, $M_1 = 0.32, M_2 = 0.18$. $N_l = 20$.

$\boldsymbol{\ell} = (l, m, n)$	$k_{N,\boldsymbol{\ell}}$ [1/m]	$k_{\text{exact},\boldsymbol{\ell}}$ [1/m], , $\hat{h} = 0$	$k_{\text{iter},\boldsymbol{\ell}}$ [1/m]	$f_{\text{iter},\boldsymbol{\ell}}$ [Hz]	$Z_2^*(f)$
$(1, 0, 0)$	8.246	$(8.175, 0.954)$	$(8.853, -0.762)$	1514.7	$(14.94, -25.58)$
$(2, 0, 0)$	16.491	$(16.350, 0.961)$	$(16.326, 0.422)$	2793.2	$(6.01, -16.45)$
$(3, 0, 0)$	24.737	$(24.527, 0.973)$	$(24.528, -0.012)$	4196.4	$(3.45, -11.43)$

Table 7: CVRC chamber frequency [Hz] of the first mode.

f_{exp} [Garby, 2013]	f_{LES} [Garby, 2013]	f_{AVSP} [Garby, 2013] $M_1 = M_2 = 0$	f_{iter} $M_1 = M_2 = 0$	f_{iter} $M_1 = 0.32$, $M_2 = 0.18$
1400	1510	**1621**	**1483**	**1515**

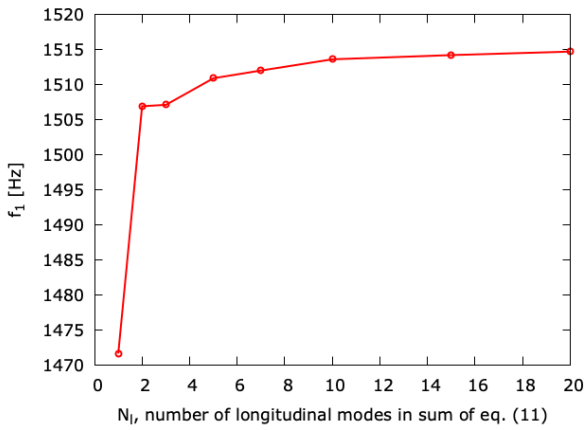

Figure 10: Convergence of iterative calculation for the first mode of CVRC with heat sources, $M_1 = 0.32, M_2 = 0.18$.

CONCLUSIONS

The objective of the paper is to predict linear thermoacoustic instabilities occurring in combustion chambers of rocket engines using an iterative method. It basically includes computation of the natural eigenmodes of the combustion chamber first, and then a corrective iterative process for determining the chamber eigenmodes and wavenumbers due to the inhomogeneities arising from the unsteady heat release in the chamber and actual conditions at its boundaries. The results for a two dimensional rectangular test geometry with impedance boundary conditions indicated good agreement with the analytical solution. The iterative computations using a literature based unsteady heat release data set for the experimental setup called CVRC indicated that reasonably good predictions could be obtained by the approach. Since thermoacoustic instability prediction requires the unsteady heat release field for a given chamber, a numerical framework for its computation employing LES is being established as part of this continuing work.

References

Candel, S. and Durox, D. and Schuller, T. (2004) *Flame interactions as a source of noise and combustion instabilities*, 10th AIAA/CEAS Aeroacoustics Conference, AIAA 2004-2928, 2004

Culick, F. E. C. and Yang, V. (1995) *Overview of combustion instabilities in liquid-propellant rocket engines*, Liquid Rocket Engine Combustion Instability. Progress in Astronautics and Aeronautics. No.169, AIAA, 1995

Culick, F.E.C. (2006) *Unsteady Motions in Combustion Chambers for Propulsion Systems*, AG-AVT-039

Evesque, S. and Polifke, W. (2002) *Low-Order Acoustic Modelling for Annular Combustors: Validation and Inclusion of Modal Coupling*, In International Gas Turbine and Aeroengine Congress & Exposition, ASME Paper, volume GT-2002-30064, 2002

Garby, Romain W. (2013) *Simulations of flame stabilization and stability in high-pressure propulsion systems*, PhD. Thesis, The University of Toulouse, 2013.

Garby, Romain W. (2013) *Large-Eddy Simulation of combustion instabilities in a variable-length combustor*, Comptes Rendus Mecanique, Vol. 341, p: 220–229, 2013.

Miller, K. J. (2005) *Experimental Study of Longitudinal Instabilities in a Single Element Rocket Combustor*, Masters Thesis, Purdue University, 2005.

Nicoud, F. and Benoit, L. and Sensiau, C. and Poinsot, T. (2007) *Acoustic modes in combustors with complex impedances and multidimensional active flames*, AIAA Journal, 45:426–441, 2007.

Pieringer, J. and Sattelmayer, T. and Fassl, F. (2009) *Simulation of Combustion Instabilities in Liquid Rocket Engines with Acoustic Perturbation Equations*, Journal of propulsion and power, 25(5):1020–1031, 2009.

Schmitt, T. and Staffelbach, G. and Ducruix, S. and Gröning and Hardi J. and Oschwald, M. (2017) *Large-Eddy Simulations of a sub-scale liquid propellant combustor: influence of fuel injection temperature on thermo-acoustic stability*, 7th European Conference for Aeronautics and Aerospace Sciences, EUCASS, 2017

Searby, G. and Rochwerger, D. (1991) *A parametric acoustic instability in premixed flames*, J. Fluid Mech. Vol 231, p:529-543, 1991

Sisco, J. C., Yu, Y. C., Sankaran, V., and Anderson, W. E. (2011) *Examination of mode shapes in an unstable model combustor*, Journal of Sound and Vibration, Vol. 330, pp. 61–74, 2011

Stow, S.R. and Dowling, A.P. (2009) *A time-domain network model for nonlinear thermoacoustic oscillations*, Journal of Engineering for Gas Turbines and Power, 131:031502, 2009

Urbano, A. and Selle, L. and Staffelbach, G. and Cuenot, B. and Schmitt, T. and Ducruix, S. and and Candel, S. (2016) *Exploration of combustion instability triggering using Large Eddy Simulation of a multiple injector liquid rocket engine*, Combustion and Flame, Vol. 169, pp. 129–140, 2016.

Yu, Yen Ching (2009) *Experimental and Analytical Investigations of Longitudinal Combustion Instability in a Continuously Variable Resonance Combustor (CVRC)*, PhD. Thesis, Purdue University, 2009.

Yu, Y. C., O'Hara, L. A., Sisco, J. C., and Anderson, W. E. (2009) *Experimental study of high-frequency combustion instability in a continuously variable resonance combustor*, 47th AIAA Aerospace Sciences Meeting, Orlando, Florida, January 2009

Yu, Y. C. (2012) *Spontaneous Longitudinal Combustion Instability in a Continuously-Variable Resonance Combustor*, Journal of Propulsion and Power, Vol. 28 (5), pp: 876–887, 2012.